EFDA–JET–CP(08)03-13

V. Pericoli Ridolfini, Yu. Baranov, M. Beurskens, M. Brix, P. Buratti, G. Calabrò, C. Castaldo, R. Cesario, C.D. Challis, R. De Angelis, P.C. de Vries, J. Ferron, E. Giovannozzi, C. Giroud, M. Gryaznevich, T.C. Hender, D. Howell, E. Joffrin, T. Luce, P. Lomas, J. Mailloux, D.C. McDonald, J. Menard, M Murakami, F. Orsitto, F. Rimini, G. Saibene, S. Sharapov, P. Smeulders, I. Voitsekovitch, O. Zimmermann and JET EFDA contributors

High β_N Experiments at JET in ITER-Like Plasmas in Support of the ITER Steady State Scenario

High β_N Experiments at JET in ITER-Like Plasmas in Support of the ITER Steady State Scenario

V. Pericoli Ridolfini[1], Yu. Baranov[2], M. Beurskens[2], M. Brix[2], P. Buratti[1], G. Calabrò[1], C. Castaldo[1], R. Cesario[1], C.D. Challis[2], R. De Angelis[1], P.C. de Vries[2], J. Ferron[3], E. Giovannozzi[1], C. Giroud[2], M. Gryaznevich[2], T.C. Hender[2], D. Howell[2], E. Joffrin[4], T. Luce[3], P. Lomas[2], J. Mailloux[2], D.C. McDonald[2], J. Menard[5], M Murakami[6], F. Orsitto[1], F. Rimini[4], G. Saibene[7], S. Sharapov[2], P. Smeulders[1], I. Voitsekovitch[2], O. Zimmermann[8] and JET EFDA contributors*

JET-EFDA, Culham Science Centre, OX14 3DB, Abingdon, UK

[1]Associazione Euratom-ENEA sulla Fusione, C. R. Frascati, C.P. 65, 00044-Frascati, Italy
[2]EURATOM-UKAEA Fusion Association, Culham Science Centre, OX14 3DB, Abingdon, OXON, UK
[3]General Atomics, P.O.Box 85608, San Diego, CA 92186-5608, California, USA
[4]Association EURATOM-CEA, DSM/DRFC, Cadarache, F-13108 Saint Paul Lez Durance, France
[5]Princeton Plasma Physics Laboratory, James Forrestal Campus, Princeton, NJ 08543, New Jersey, USA
[6]Oak Ridge National Laboratory, Oak Ridge, TN 37831-6169, Tennessee, USA
[7]EFDA CSU-Garching, Germany
** See annex of M.L. Watkins et al, "Overview of JET Results ", (Proc. 21 st IAEA Fusion Energy Conference, Chengdu, China (2006)).*

Preprint of Paper to be submitted for publication in Proceedings of the
35th EPS Conference on Plasma Physics, Hersonissos, Crete, Greece
(9th June 2008 - 13th July 2008)

INTRODUCTION

Low tokamak plasma current, I_p, favours steady-state operation, due to the smaller Non-Inductive (NI) current to be externally driven, and to the higher self-generated bootstrap current fraction I_{bs}/I_p, for a given plasma pressure. However, this penalizes the energy confinement time τ_E ($\propto I_p$), as compared to the basic H-mode value $\tau_{98(y,2)}$[1]. Advanced tokamak scenarios aim at compensating for this τ_E drop, in order to preserve a high fusion gain (Q~5). The last JET campaigns began to study the way to approach the ITER main targets, which are $H_{98} \equiv \tau_E/\tau_{98(y,2)}$~1.5 and β_N~3. β_N is given by $\beta_N = \beta_T B_T a/I_p$ (β_T = thermal to toroidal magnetic pressure ratio, B_T = magnetic field, a=plasma minor radius) and characterises both the fusion performance and the NI operation [2]. The two main issues of high confinement and of stability have been studied by developing two different scenarios, both with an ITER-like plasma shape (high triangularity δ~0.45, safety factor q_{95}~5). The first one, B_T/I_p = 2.3T/1.5MA, aims at raising τ_E by exploiting the improved core confinement produced by an Internal Transport Barrier (ITB). The second scenario, B_T/I_p = 1.8T 1.2MA, instead aims at producing high β_N values without ITBs in order to minimize the effect of steep pressure gradients on stability. This same reason and the risk of impurity accumulation limit also the acceptable gradients strength in ITBs.

PROGRESS OF THE SCENARIOS

The main external power source is the neutral beam injection (NBI, P_{NBI} up to 21MW). In the ITB case the RF power has also been used: ion cyclotron resonance heating (ICRH, P_{ICRH} up to 7MW) and lower hybrid (LH, P_{LH} up to 2.5MW). LH has been mainly exploited in the very early phase of the discharge to explore different target qprofiles for the main, NBI-heated, phase. Discharge optimization also required testing different NBI waveforms, I_p ramp-up rates, and, for ITBs, plasma shapes in the divertor region. Between the two tested shapes, the better performing (N.2) has the X-point farther from the inner divertor plate and strike-point closer to the pumping duct. It is also less sensitive to the NBI timing, shows more regular ELMs and a better impurity pumping capability.

The present data are compared with the various JET scenarios in figs. 1 and 2. Figure 1 is the plot of β_N versus the pressure profile peaking parameter $p_0/\langle p \rangle$. Onto this plane the β_N stability domain is usually represented. The new data, selected among those lasting at least $10\tau_E$, clearlymove forwards a better stability, i.e. higher β_N and low $p_0/\langle p \rangle$. Figure 2 instead plots the achieved β_N values versus the Greenwald density fraction $\bar{n}_e/n_{GW}$ for the ITB scenario ($\bar{n}_e$ = line averaged density, $\bar{n}_{GW} = I_p/(\pi a^2)$ [10^{20} m^{-3}, MA, m^2]). The progress made in the route towards the ITER target, $n_e \sim 0.8 \cdot n_{GW}$, with respect to the previous low-δ data is illustrated by this graph. Non-degraded performance is achieved at the highest density ($\bar{n}_e = 0.45 \cdot 10^{20}$ m^{-3}).

The two scenarios, 'ITB' and''No-ITB', are compared in Fig.3, by plotting the maximum β_N, reached during the first 3s after the NBI start, versus qmin, minimum of the target q(r). The β_N data are averaged over 0.5s, q_{min} over 1s. The q profile is taken from the reconstructed equilibrium constrained with MSE (Motional Stark Effect) and kinetic pressure data. Additional consistency is

imposed by the radii of the MHD activities that the mode analysis unequivocally identifies. These can be Alfven cascades, fishbone-like activity on the q = 2 surface, or modes with recognized poloidal and toroidal numbers (m,n). In either case, a wide, large n = 1 MHD mode often terminates the high β_N phase. The 'No-ITB' values here plotted all end this way. Stable discharges have β_N only ~10% lower, on average. Both cases are plotted for ITB discharges, those free from the big n = 1 mode and lasting as long as the main heating pulse (~$10\tau_E$) are indicated by full symbols. This MHD activity is recognized mostly as a tearing mode (with m = 2) [3] with often an ideal internal kink as a precursor. The β_N at which it starts growing rapidly is typically 20% higher than the critical value derived from the technique of the resonant field amplification [4]. For the ITB case, the evolution of the q(r) profiles, reconstructed as outlined before, shows that the mode is strongly destabilized when a wide region with shear ~0 and q~2 develops, in ~1-3s time. The formation of a broad shearless region is consistent also with the 'No-ITB' data, as suggested by the same nature of the mode and by the presence of the very critical qmin~2 surface, which can strongly reduce the β_N threshold for destabilization. Consistently again, the very recent data obtained at q_{min} >2 and s≤0, display again a β_N value >3. Its short life is due to the little time needed to reach again the nearby critical q-profile shape. The lack of a dangerous β_N for the ITBs at q_{min} ~2 is quite evident if we restrict to cases when an e-ITB develops, see Fig.3. It is due to a definitely more reversed shear of the target that takes longer do evolve into an instable shape. The link between q(r) and the e-ITB is further discussed below.

The confinement follows the β_N behaviour in both scenarios. In No-ITB case H98 reaches ~1.2 for the lowest q_{min}, it is about 1-1.1 for most points, then drops down to 0.8 for q_{min} ~2. In the ITB case, H98 increases almost linearly up to the value of 1.1, fig. 4. It should also be stressed that an additional 30% of energy is stored in suprathermal particles and that in most cases the LH power is absorbed only in the very peripheral and poorly confining region. This is supported by the absence of suprathermal electrons, by the fact that the LH power during the main heating does not affect any core parameter within the measurement errors, by code calculations and by a previous work on JET [5]. By excluding the LH power, H98 would attain 1.2.

Finally, the NI current fraction is up to 75%, ~40% bootstrap and 30% NB-driven. However, the residual ohmic current is still high enough to affect considerably the q(r) profile. Then, a full alignment of the NI current radial profile with that required to sustain steadily the high β_N phase has yet to be definitely proved, despite the long durations so far established (up to $30\tau_E$).

THE EFFECT OF THE RADIAL PROFILES

Stationarity and stability can be affected by the pressure and current profiles, as shown above, whereas core confinement is characterized by the magnitude of the gradients. The ITB case is more suited for a dedicated analysis because of the wider range of $\nabla T(e^-$ and $i^+)$. The data so far collected suggest that e-ITB plays a primary role in the confinement. The plot of the β_N values versus ρ^*_T (i^+ and e^-), fig.5, shows that the most confining discharges have the strongest e-ITBs. ρ^*_T is a normalized

∇T, defined as $\rho^*_T = \rho_L/L_T$ (ρ_L = ion Larmor radius at the sound velocity, $L_T = T/\nabla T$) and measures the ITB strength. The following is derived: 1) β_N saturates for high values of $\rho^*_{T,i}$ (void symbols) at different levels for the two plasma shapes; 2) an e–ITB (full symbols) usually develops in shape N.2 and does not in shape N.1; 3) β_N increases continuously with $\rho^*_{T,e}$. This dependence shows that strengthening an e–ITB offers a very good opportunity to increase β_N.

The e– barrier features are in turn closely linked the q(r) shape. The ITB steepest gradient is indeed anchored to the radius where q = 2, as shown in fig.6 by the plot of the radius of $\rho^*_{Te,Max}$ versus R(q = 2). This latter is inferred from the local perturbation on $T_e(r)$ (±1cm) induced by the MHD fishbone activity. A local shear s ~ 0 is also needed to form the ITB. Indeed, an s < 0 implies a second q = 2 surface, which then drives easily double tearing instabilities, whereas s > 0 and large is the usual non-ITB situation. However, cases with small but positive shear are found, though s < 0 usually produces a stronger ITB. Since the i+ITB radius is closely related to the e-ITB, even though normally a bit larger, producing wider ITBs with $q_{95} \sim 5$ should be extremely difficult. By comparing discharges equal but for the use of LHCD in preparing the q(r) target is also made clear that the condition s < 0 is not sufficient. With LHCD the ITB onset and the appearance of q = 2 are significantly delayed (~ 4s), consistently with a q(r) initially more reversed and slower diffusing.

ACKNOWLEDGEMENT

This work, supported by the European Community under the EURATOM/ENEA contract of Association, was carried out within the framework of the European Fusion Development Agreement. The views and opinions expressed herein do not necessarily reflect those of the European Commission.

REFERENCES

[1]. E.J. Doyle et al., Nucl. Fusion **47** (2007) S18–S127

[2]. X. Litaudon et al., *Plasma Phys. Control. Fusi*on, **V. 48** (2006), p. A1–A34

[3]. P. Buratti et al. ‘Radial analysis of beta-limiting modes in JET’ this conference

[4]. M. Gryaznevich ‘Beta limit in JET’, this conference

[5]. V. Pericoli Ridolfini et al., *Plasma Phys. Controll. Fusion*, **V. 39**, p. 1115-1128

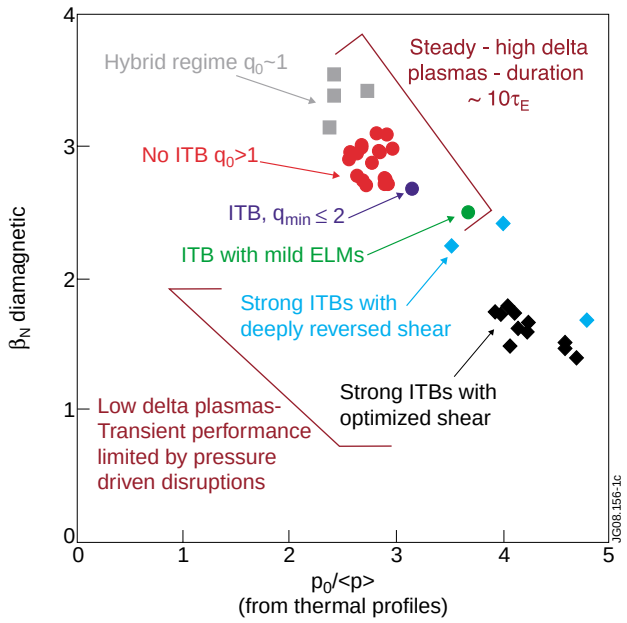

Figure 1: Plot of β_N (diamagnetic) versus profile peaking p_0/<p>.

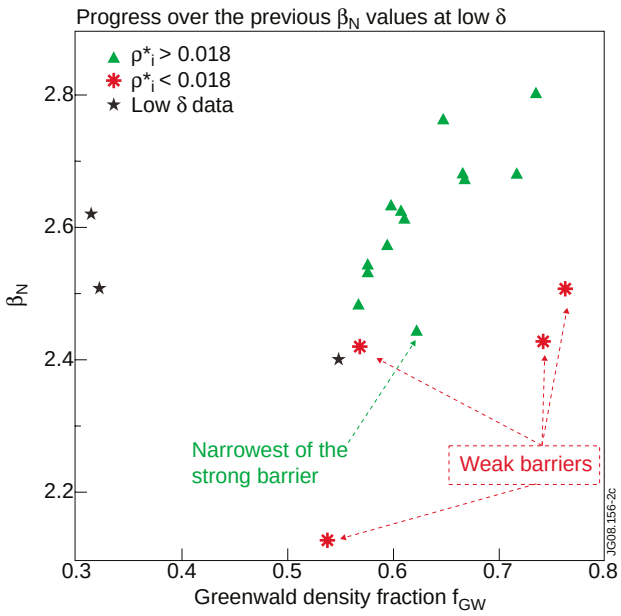

Figure 2: Plot of β_N (diamagnetic) versus $\bar{n}_e/n_{GW}$.

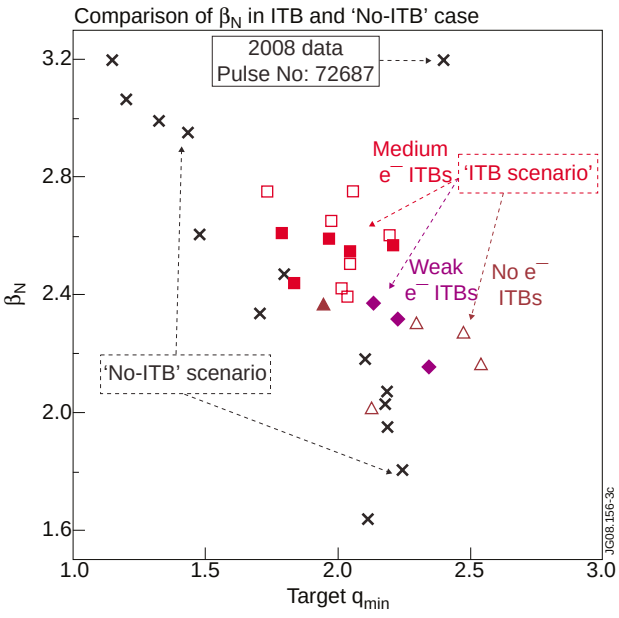

Figure 3: Plot of β_N (diamagnetic) versus the target q_{min}.

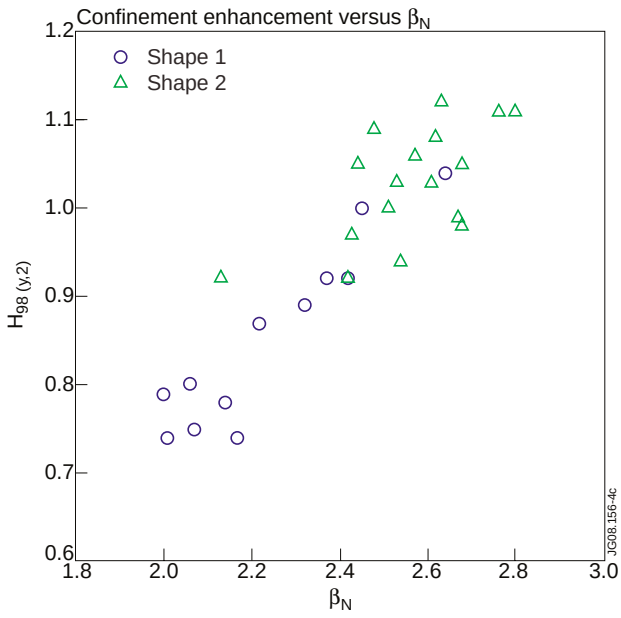

Figure 4: Plot of the confinement enhancement versus β_N (diamagnetic)

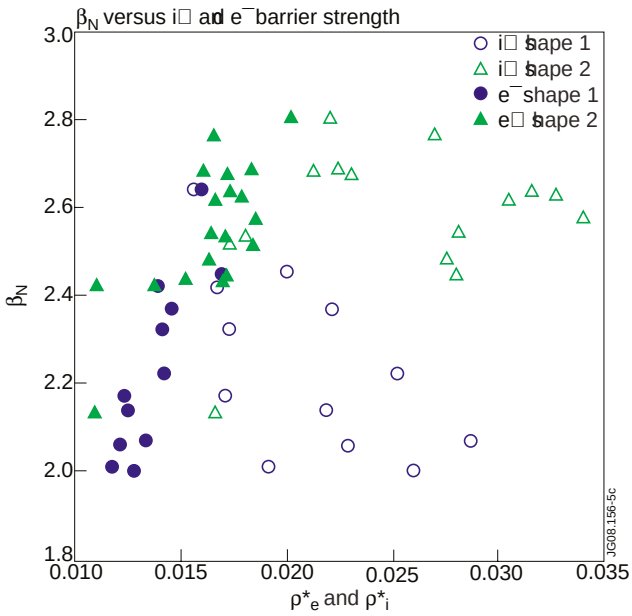

Figure 5: Plot of β_N (diamagnetic) versus the e- and i+ ITB strength

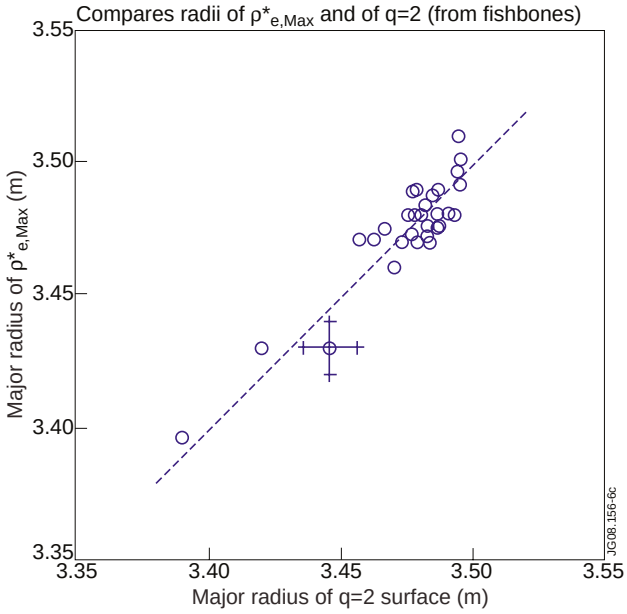

Figure 6: Plot of the ITB radius versus the e- fishbones radius